Journal of Solid State Chemistry 183 (2010) 1536–1544

Contents lists available at ScienceDirect

Journal of Solid State Chemistry

journal homepage: www.elsevier.com/locate/jssc

# Electronic structure of ZrCuSiAs and ZrCuSiP by X-ray photoelectron and absorption spectroscopy

Peter E.R. Blanchard, Ronald G. Cavell, Arthur Mar *

*Department of Chemistry, University of Alberta, Edmonton, Alberta, Canada T6G 2G2*

ARTICLE INFO

*Article history:*
Received 22 February 2010
Received in revised form
21 April 2010
Accepted 24 April 2010
Available online 14 May 2010

*Keywords:*
XPS
XANES
Quaternary pnictides

ABSTRACT

The electronic structures of quaternary pnictides ZrCuSi*Pn* (*Pn*=P, As) were analyzed by X-ray photoelectron spectroscopy (XPS) and X-ray absorption near-edge spectroscopy (XANES). Shifts in the core-line XPS and the XANES spectra indicate that the Zr and Cu atoms are cationic, whereas the Si and *Pn* atoms are anionic, consistent with expectations from simple bonding models. The Cu 2*p* XPS and Cu L-edge XANES spectra support the presence of $Cu^{1+}$. The small magnitudes of the energy shifts in the XPS spectra suggest significant covalent character in the Zr–Si, Zr–*Pn*, and Cu–*Pn* bonds. On progressing from ZrCuSiP to ZrCuSiAs, the Si atoms remain largely unaffected, as indicated by the absence of shifts in the Si $2p_{3/2}$ binding energy and the Si L-edge absorption energy, while the charge transfer from metal to *Pn* atoms becomes less pronounced, as indicated by shifts in the Cu K-edge and Zr K, L-edge absorption energies. The transition from two-dimensional character in LaNiAsO to three-dimensional character in ZrCuSiAs proceeds through the development of Si–Si bonds within the [ZrSi] layer and Zr–As bonds between the [ZrSi] and [CuAs] layers.



## 1. Introduction

The tetragonal structure of ZrCuSiAs (space group *P*4/*nmm* (no. 129)) serves as the prototype for numerous compounds, with over 150 representatives [1]. By far the two largest subsets are the rare-earth transition-metal pnictide oxides *REMPn*O [2], which are superconductors at relatively high temperatures when doped with fluorine [3–5], and the rare-earth copper chalcogenide oxides *RE*Cu*Ch*O, which are promising transparent p-type semiconductors [6]. It has been fashionable to portray the structure of the pnictide oxides in terms of a stacking of alternating [*RE*O] and [*MPn*] layers, with both O and *M* atoms in tetrahedral coordination geometries (Fig. 1a). In contrast, there are only three examples of quaternary silicon pnictides known so far: ZrCuSiAs itself, HfCuSiAs, and ZrCuSiP [7,8]. Ostensibly the structure of ZrCuSiAs can also be described in terms of layers, [ZrSi] and [CuAs], with Si and Cu atoms in the tetrahedral sites (Fig. 1b). The *c*/*a* ratio is 2.0–2.3 for all the oxide representatives of this structure type, but 2.6 for the three quaternary silicon pnictides [1]. Paradoxically, this expanded *c*/*a* ratio does not mean that the layers are further apart in ZrCuSiAs! The reasons seem evident even from just casual inspection of the figures. Within individual layers, the tetrahedra are highly compressed along the *c*-direction in *REMPn*O, but highly elongated in ZrCuSiAs. This distortion causes the Zr atoms in the [ZrSi] layer to approach the As atoms in the [CuAs] layer quite closely (2.8 Å) [7]. The electron-precise formulations $[RE^{3+}O^{2-}][M^{2+}Pn^{3-}]$ and $[Zr^{4+}Si^{2-}][Cu^{1+}As^{3-}]$, deduced upon the assumption of full electron transfer, seem to provide a tidy explanation for the origin behind this distortion. Apart from the transition-metal atoms which can support partially filled *d*-states, all atoms in *REMPn*O attain filled-shell electron configurations; thus, *REMPn*O (and the other oxides) are classified as "normal valence" compounds. On the other hand, the Si atoms in ZrSiCuAs are deficient with respect to the 8–*n* rule and must then form Si–Si bonds; that is, ZrCuSiAs should be considered a polyanionic compound. The formation of these Si–Si bonds contracts the structure within the *ab* plane, concomitant with an expansion along the *c*-direction.

In view of these profound differences, it is worthwhile to re-examine the electronic structure and bonding in ZrCuSiAs, as well as its phosphide analogue ZrCuSiP. We take primarily an experimental approach, applying X-ray photoelectron spectroscopy (XPS) and X-ray absorption near-edge spectroscopy (XANES) to probe energy differences in core-level atomic states, supplemented by band structure calculations to examine the bonding character in these compounds. The results are compared with LaNiAsO, a representative member studied in our previous investigations of rare-earth arsenide oxides [9].

## 2. Experimental

### 2.1. Synthesis

ZrCuSiAs and ZrCuSiP were prepared according to literature procedures [7,8]. Reagents were Zr wire (99.9%, A.D. Mackay), Cu

* Corresponding author. Fax: +1 780 492 8231.
*E-mail address:* arthur.mar@ualberta.ca (A. Mar).

0022-4596/$ - see front matter © 2010 Elsevier Inc. All rights reserved.
doi:10.1016/j.jssc.2010.04.032

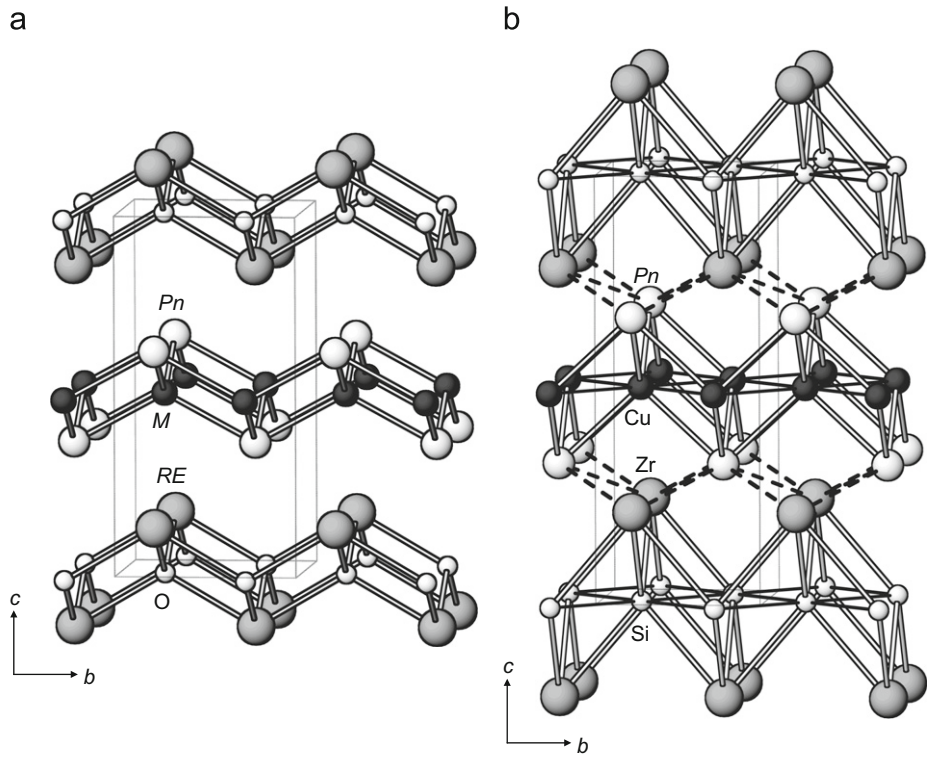


**Fig. 1.** Crystal structure of (a) *REMPn*O showing non-interacting [*RE*O] and [*MPn*] layers and (b) ZrCuSi*Pn* (*Pn*=P, As) showing interacting [ZrSi] and [Cu*Pn*] layers, stacked along the *c*-direction.

powder (99.9999%, Cerac), Si pieces (99.99999%, Alfa-Aesar), As powder (99.5%, Cerac), and red P powder (99.995%, Cerac). For ZrCuSiAs, a stoichiometric mixture of "ZrSi" (previously prepared by arc-melting), Cu, and As powders was placed within an evacuated sealed fused-silica tube, which was heated to 873 K over 1 day, kept at that temperature for 2 days, heated to 1173 K over 1 day, kept at that temperature for 2 days, and water-quenched. The product was reground and reheated at 1073 K for 4 days; this procedure was repeated three times. For ZrCuSiP, a stoichiometric mixture of "ZrCuSi" (previously prepared by arc-melting) and P was placed within an evacuated sealed fused-silica tube, which was heated to 873 K over 1 day, kept at that temperature for 1 day, heated to 1123 K over 1 day, kept at that temperature for 2 days, and water-quenched. The product was reground and reheated at 1123 K for 4 days; this procedure was repeated three times. The products were judged to be single-phase from their powder X-ray diffraction patterns collected on an Inel powder diffractometer (Fig. S1 in Supplementary Data). The unit cell parameters are $a=3.6608(8)$ Å and $c=9.604(2)$ Å for ZrCuSiAs, and $a=3.5663(8)$ Å and $c=9.421(2)$ Å for ZrCuSiP, which are comparable to previously reported values ($a=3.6736(2)$ Å and $c=9.5712(9)$ Å for ZrCuSiAs [7]; $a=3.5671(1)$ Å and $c=9.4460(4)$ Å for ZrCuSiP [8]).

### 2.2. XPS analysis

XPS spectra for ZrCuSiAs and ZrCuSiP were measured on a Kratos AXIS 165 spectrometer equipped with a monochromatic Al $K\alpha$ X-ray source (14 mA, 15 kV) and a hybrid lens with a spot size of $700 \times 400\ \mu m^2$. The samples are air-stable but to minimize exposure to air, they were handled in an Ar-filled glove box where they were finely ground, pressed into In foil, mounted on a Cu sample holder, and placed in a sealed container for transfer to the analysis chamber of the spectrometer. The pressure inside the XPS instrument was maintained between $10^{-7}$ and $10^{-9}$ Pa. Samples were sputter-cleaned with an $Ar^+$ ion beam (4 kV, 10 mA) until core-line peaks associated with surface oxides were no longer observed in the XPS spectra. A small shoulder in the As 3*d* XPS spectra indicated that a slight reduction of As occurred in ZrCuSiAs; however, the binding energies (BE) in these and other spectra were, within standard uncertainties, the same before and after the sputtering procedure.

Survey spectra, collected with a BE range of 0–1100 eV, a pass energy of 160 eV, a step size of 0.7 eV, and a sweep time of 180 s, confirmed the expected chemical compositions (Zr:Cu:Si:*Pn*=1:1:1:1) for the samples examined. High-resolution core-line spectra were collected with an energy envelope of appropriate range (50 eV for Zr 3*d*; 60 eV for Cu 2*p*; 20 eV for Si 2*p*, As 3*d*, and P 2*p*), a pass energy of 20 eV, a step size of 0.05 eV, and a sweep time of 180 s. No charge correction was required because the samples are good conductors. The spectra were calibrated to the C 1*s* line at 284.8 eV arising from adventitious carbon. As a check, another suitable calibration technique is to set the first derivative of the edge onset of the valence band, which should be at 0 eV for a metallic sample [10]. The spectra were analyzed with use of the CasaXPS software package [11]. The background arising from energy loss was removed by applying a Shirley-type function and the peaks were fitted to pseudo-Voigt (70% Gaussian and 30% Lorentzian) line profiles to take into account spectrometer and lifetime broadening effects. Table 1 lists average BE values expressed to two decimal places, with uncertainties estimated at better than $\pm 0.10$ eV, as established by collecting multiple spectra (Table S1 in Supplementary Data).

### 2.3. XANES analysis

X-ray absorption spectra were measured at the Canadian Light Source (CLS) in Saskatoon, Saskatchewan. The bending magnet soft X-ray microcharacterization beamline (SXRMB, 06B1-1) was used for Zr L-edge spectra, the high-resolution spherical grating

**Table 1**
Core-line BEs (eV) for ZrCuSiAs and ZrCuSiP.

| | ZrCuSiAs | ZrCuSiP |
|---|---|---|
| Zr $3d_{5/2}$[a] | 179.64(2) | 179.66(5) |
| Cu $2p_{3/2}$[a] | 933.68(3) | 933.70(6) |
| Si $2p_{1/2}$ | 99.41(4) | 99.40(5) |
| As $3d_{5/2}$ or P $2p_{3/2}$ | 41.13(6) | 128.82(6) |

[a] For comparison, the Zr $3d_{5/2}$ BE is 178.91(3) eV in Zr metal and the Cu $2p_{3/2}$ BE is 932.86(4) eV in Cu metal.

monochromator beamline (SGM, 11ID-1) for Cu L-edge spectra, and the variable line spacing plane grating monochromator beamline (VLS PGM, 11ID-2) for Si L-edge spectra. The SXRMB beamline is equipped with an InSb (111) double crystal monochromator which provided a photon flux of $\sim 10^{11}$ photons/s, with a resolution of 3.3 eV at 10 keV and a beamsize of approximately $300 \times 300\,\mu m^2$. Finely ground samples were mounted on carbon tape and inserted into the vacuum chamber via a load lock. Multiple scans of the Cu and Si L-edge XANES spectra were collected for each sample, giving an estimated accuracy of $\pm 0.1$ eV for the absorption energies. Spectra were collected in total electron yield (TEY) and X-ray fluoresence yield (FLY) modes, with a step size of 0.1 eV through the edge over various energy ranges (Zr L-edge, $\sim$50 eV below to $\sim$500 eV above the edge; Cu L-edge, $\sim$20 eV below to $\sim$65 eV above; Si L-edge, $\sim$30 eV below to $\sim$30 eV above). The Zr spectra were calibrated against a standard of $FePO_4$, with the maximum of the first derivative of the P K-edge set to 2153.0 eV [12]; the Cu and Si spectra were calibrated against standards of the elemental metals, with the maxima in the first derivatives of the $L_3$-edges set to 932.7 eV for Cu and 99.2 eV for Si [13]. Uncertainties of $\pm 0.1$ eV for the absorption edge energies were estimated by collecting multiple scans for each sample.

The Pacific Northwest Consortium/X-ray Operations and Research Collaborative Access Team (PNC/XOR-CAT), Sector 20 bending magnet beamline (20-BM), at the Advanced Photon Source (APS) at Argonne National Laboratory was used to measure Zr and Cu K-edge XANES spectra. The silicon (111) double crystal monochromator on this beamline provided a photon flux of $\sim 10^{11}$ photons/s with a resolution of 1.4 eV at 10 keV and a beam size of approximately $1 \times 4.5\,mm^2$. Finely ground samples were sandwiched between Kapton tape and positioned at 45° to the X-ray beam. Spectra were measured in transmission mode with an ionization detector (filled with a 50:50 mixture of He and $N_2$ in the ionization chamber) and in fluorescence mode with a Canberra 13-element fluorescence detector. The step size was 0.1 eV through the absorption edge. Standards of Zr or Cu metal were placed in a second position downstream of the samples and measured in transmission mode concurrently with the samples. The maxima in the first derivatives of the K-edges were set to 17,998 eV for Zr and 8979 eV for Cu [13]. All XANES spectra were analyzed with use of the Athena software program [13].

### 2.4. Band structure calculations

Tight-binding linear muffin tin orbital (TB-LMTO) band structure calculations were performed on ZrCuSiAs and ZrCuSiP within the local density and atomic spheres approximations using the Stuttgart TB-LMTO program [14]. The basis sets consisted of Zr 5*s*/5*p*/4*d*/4*f*, Cu 4*s*/4*p*/3*d*, Si 3*s*/3*p*/3*d*, As 4*s*/4*p*/4*d*, and P 3*s*/3*p* orbitals, with the Zr 4*f*, Si 3*d*, and As 4*d* orbitals being downfolded. Integrations in reciprocal space were carried out with an improved tetrahedron method over 84 independent *k* points within the first Brillouin zone. For comparison, the band structure of LaNiAsO was also calculated in a similar manner.

## 3. Results and discussion

To parallel the approach taken previously to analyze the electronic structure of the rare-earth arsenide oxides *REMAsO*, we first break down the structure of ZrCuSi*Pn* (*Pn*=P, As) into its nominally separate "layers", [ZrSi] and [Cu*Pn*]. Then we examine the question of whether the layers interact by probing to what extent charge transfer occurs within and between these layers.

### 3.1. [ZrSi] layer

The Zr 3*d* XPS spectra for ZrCuSiAs and ZrCuSiP were fitted to two peaks corresponding to the spin–orbit-split $3d_{5/2}$ and $3d_{3/2}$ final states, in an intensity ratio of 3:2 (Fig. 2). (The weak shoulder found at high BE in all spectra is interpreted as a surface oxide.) The Zr $3d_{5/2}$ BEs in ZrCuSiAs (179.64(2) eV) and ZrCuSiP (179.66(5) eV) are higher than in Zr metal (178.91(3) eV) [15], indicating the presence of cationic Zr atoms, but they are much lower than in $ZrO_2$ (182.7(6) eV) [15], indicating that the charge is nowhere as extreme as 4+ which would be expected if full electron transfer were to occur. Indeed, a signature for electronic delocalization is already evident in the asymmetric line shapes of these peaks, skewed towards higher BE. Common in the spectra of many elemental transition metals, including Zr, this asymmetry arises when valence electrons, interacting with the core–hole formed after photoionization, are excited into the continuum of

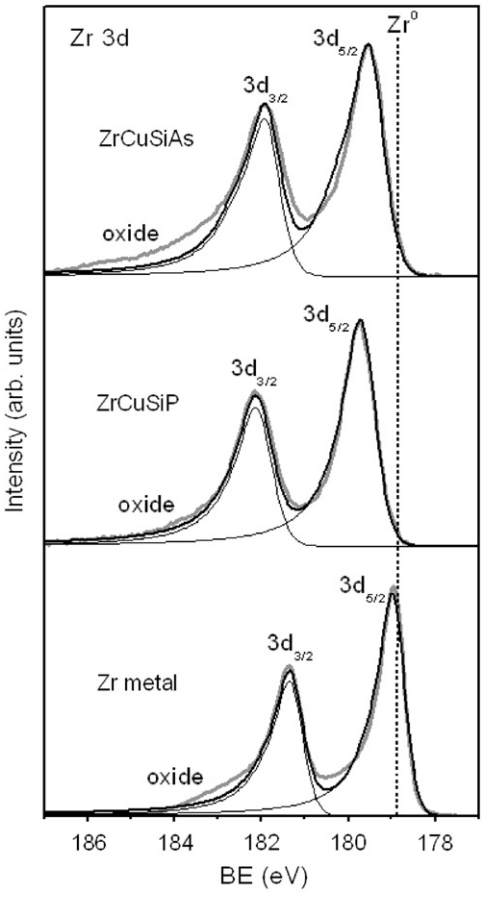


**Fig. 2.** Zr 3*d* XPS spectra, fitted with $3d_{5/2}$ and $3d_{3/2}$ components, for ZrCuSiAs, ZrCuSiP, and Zr metal. The vertical dashed line marks the $3d_{5/2}$ BE for Zr metal.

empty conduction states above the Fermi edge [16]. In this way, the core electrons experience substantial nuclear screening to the extent that the Zr 3*d* BEs in ZrCuSiAs and ZrCuSiP do not shift much from that in Zr metal. Further evidence for this electronic delocalization is provided by resistivity measurements, which show semimetallic behaviour for ZrCuSiP [8], and band structure calculations, which show a pseudogap at the Fermi level (vide infra).

The Si 2*p* XPS spectra were fitted to two components representing the $2p_{3/2}$ and $2p_{1/2}$ spin–orbit-split final states, in an intensity ratio of 2:1, FWHM of 0.9 eV, and an energy splitting of 0.6 eV (Fig. 3a). (The second set of peaks at higher BE is assigned to surface silicon suboxides [17,18].) Surprisingly, the Si $2p_{3/2}$ BEs in ZrCuSiAs (99.41(4) eV) and ZrCuSiP (99.40(5) eV) are, within standard uncertainty, the same as in elemental Si (99.5(2) eV) [15,17], even though the formal charge is 2−. A closely related case is $Zr(As_{0.6}Si_{0.4})As$, in which the more perceptibly shifted Si $2p_{3/2}$ BE (98.9 eV) is correlated with an approximate negative charge of 1− [18]. The implication is that the Zr–to–Si charge transfer is less pronounced and that the Zr–Si bonds are even more highly covalent in ZrCuSiAs and ZrCuSiP than in $Zr(As_{0.6}Si_{0.4})As$. The absence of a BE shift would also be consistent with the occurrence of strong Si–Si bonding within square nets in the structure, supporting the presence of an extended polyanionic Si network. The identical BEs in ZrCuSiAs and ZrCuSiP suggest that the Si charges are independent of the nature of the pnicogen. To confirm this point, the Si L-edge XANES spectra, which are less sensitive to final state effects than are XPS spectra [19], were analyzed (Fig. 3b). The features (A–E) in these spectra arise from dipole-allowed transitions of 2p electrons into unoccupied s and d states ($\Delta l = \pm 1$) and are characteristic of tetrahedrally coordinated Si (such as in α-quartz) [20]. Peaks A and B correspond to transitions from 2*p* to 3*s* states (with $a_1$ symmetry); they are split 0.6 eV apart from spin–orbit-coupling into $2p_{3/2}$ ($L_3$-edge) and $2p_{1/2}$ states [20]. As anticipated, the L-edge absorption energies are essentially identical for both ZrCuSiAs and ZrCuSiP. Peak C is assigned to a $t_2 \rightarrow t_2^*$ (2*p* to strongly hybridized *s*–*p* states) transition, peak D to multiple scattering resonance (MSR), and peak E to a $2p \rightarrow 3d$ transition (or possibly a surface oxide) [20,21].

### 3.2. [CuPn] layer

The Cu 2*p* XPS spectra for ZrCuSiAs and ZrCuSiP consist of $2p_{3/2}$ and $2p_{1/2}$ core-line peaks in an intensity ratio of 2:1 (Fig. 4a). Interestingly, despite the expectation of $Cu^{1+}$, these spectra exhibit features characteristic of both $Cu^{2+}$ and $Cu^{1+}$ systems. On one hand, the Cu $2p_{3/2}$ BEs in ZrCuSiAs (933.68(3) eV) and ZrCuSiP (933.70(6) eV) are higher than in Cu metal (932.86(4) eV). The occurrence of BE shifts relative to Cu metal is usually diagnostic for compounds containing $Cu^{2+}$ but not $Cu^{1+}$ [22–25]. On the other hand, as gauged by their FWHMs, the Cu $2p_{3/2}$ peaks in ZrCuSiAs and ZrCuSiP (1.0 eV) are much narrower than in CuO (3.2 eV) but closer to those in CuBr or CuI (1.2 eV) [26–28]. The absence of line broadening is usually diagnostic for compounds containing $Cu^{1+}$ but not $Cu^{2+}$. Significant line broadening occurs for $Cu^{2+}$ ($3d^9$) where the interaction of unpaired 3*d* electrons with 2*p* electrons after photoionization gives rise to multiplet splitting, but not for $Cu^{1+}$ ($3d^{10}$) where no such interaction can occur because of the absence of unpaired electrons [29]. These seeming contradictions can be reconciled upon realization that the bonding in these quaternary pnictides is highly covalent. Thus, the BE correlation may break down, similar to the case of the chalcogenides $Cu_2S$ and CuS, which are indistinguishable by their Cu 2*p* BEs [29]. Moreover, because these pnictides are expected to be semimetallic, the mechanism for line broadening is different. The Cu $2p_{3/2}$ peaks actually resemble more closely those in Cu metal (FWHM of 0.8 eV), $CeCu_4Al$ (FWHM of 1.0 eV) [30], and other alloys containing $Cu^{1+}$ or $Cu^0$ [25], with a small asymmetry to higher BE arising in the same way (Doniach–Šunjić process) as described earlier for the Zr 3*d* peaks.

Another defining feature that can be examined is an intense satellite above the $2p_{3/2}$ core line at 940–945 eV seen in the Cu 2*p* XPS spectra for $Cu^{2+}$ but not $Cu^{1+}$ or $Cu^0$ systems [22–24,29], as has been exploited to identify $Cu^{2+}$ in cuprate superconductors [26,31–37]. The two theories developed (a "shake-up" process in which Cu valence electrons are excited into empty ligand states above the Fermi edge after photoionization [24,29], or a "shake-down" process in which ligand electrons relax into empty conduction states after photoionization [29]) both predict that this satellite is only possible in $Cu^{2+}$ systems where empty 3*d*

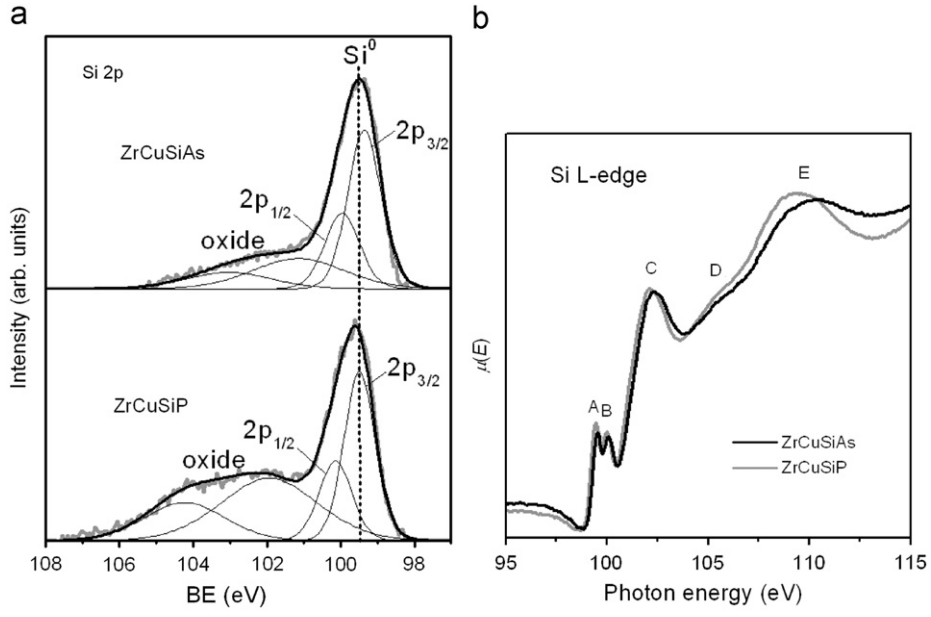


**Fig. 3.** (a) Si 2*p* XPS spectra, fitted with $2p_{3/2}$ and $2p_{1/2}$ components, and (b) Si L-edge XANES spectra (FLY mode) for ZrCuSiAs and ZrCuSiP. The vertical dashed line in (a) marks the $2p_{3/2}$ BE for elemental Si. Features A–E in (b) are discussed in Section 3.1.

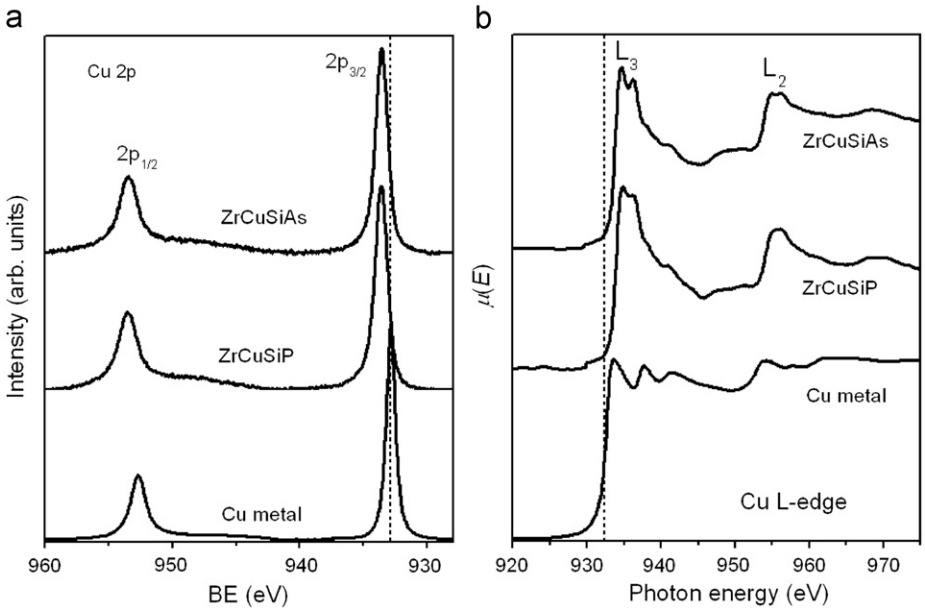


**Fig. 4.** (a) Cu 2*p* XPS spectra and (b) Cu L-edge XANES spectra (FLY mode) for ZrCuSiAs, ZrCuSiP, and Cu metal. The vertical dashed lines mark the Cu $2p_{3/2}$ BE in (a) and the Cu $L_3$-edge absorption energy in (b) for Cu metal. Spectra are offset for clarity.

conduction states are available. The absence of this satellite in ZrCuSiAs and ZrCuSiP thus eliminates the possibility for an assignment of $Cu^{2+}$.

Further information can be gained from the Cu L-edge XANES spectra, which reveal dipole-allowed transitions from $2p_{3/2}$ ($L_3$-edge) or $2p_{1/2}$ ($L_2$-edge) states to unoccupied 4*s* and 3*d* states (Fig. 4b). The lineshapes are typical of $Cu^{1+}$ compounds. Given the $d^{10}$ configuration for $Cu^{1+}$ and $Cu^0$, the $2p \rightarrow 4s$ transition is much more probable than the $2p \rightarrow 3d$ transition, whereas the reverse holds for $Cu^{2+}$ ($3d^9$) [38]. The correlation between absorption energy and charge is not so straightforward. Although it is true that the $L_3$-edge energy for $Cu^{1+}$ is higher than for $Cu^0$ because of the greater positive charge, it is actually lower for $Cu^{2+}$ because of the presence of unfilled 3*d* states [38]. The $L_3$-edge absorption energy in ZrCuSiAs and ZrCuSiP (both 934.0 eV) is found to be higher than in Cu metal (932.7 eV), supporting the presence of $Cu^{1+}$. In principle, the intensity of the Cu L-edge, which should be proportional to the number of conduction states, can be analyzed; however, this relationship is not valid here because these spectra were measured in FLY mode, which is influenced by self-absorption effects.

The As 3*d* and P 2*p* XPS spectra each show one broad signal, fitted to the As $3d_{5/2}$ and $3d_{3/2}$ components (intensity ratio of 3:2, FWHM of 0.9 eV, splitting of 0.7 eV) and P $2p_{3/2}$ and $2p_{1/2}$ components (intensity ratio of 2:1, FWHM of 0.7 eV, splitting of 0.9 eV), respectively (Fig. 5). The As XPS spectrum shows a small asymmetry at higher BE which is attributed to surface oxides (as seen in the Zr XPS spectrum, as well as in $As_{1-x}Se_x$ [39]) or may be caused by the line-broadening mechanism described earlier involving electronic delocalization in ZrCuSiAs. The P XPS spectrum includes a minor component which is assigned to the $2p_{1/2}$ core-line peak of trace amounts of elemental P, with the $2p_{3/2}$ peak presumably buried under the more intense main peaks for ZrCuSiP. The As $3d_{5/2}$ BE is lower in ZrCuSiAs (41.13(6) eV) than in elemental As (41.7(2) eV) and the P $2p_{3/2}$ BE is lower in ZrCuSiP (128.82(6) eV) than in elemental P (130.2(3) eV) [15,17], indicating the presence of anionic pnicogen atoms in both cases. As in the case for the Si atoms within the [ZrSi] layer, these BE shifts are less extreme than expected for nominal $Pn^{3-}$ anions within the [Cu*Pn*] layer because of the substantial covalent character in the bonds. The magnitude of these shifts should reflect the degree of electron transfer within the Cu–*Pn* bonds. Interestingly, the BE shifts are less pronounced for the As atoms (ΔBE of 0.6 eV) than for the P atoms (ΔBE of 1.4 eV), implying that As is less electronegative than P. This observation contradicts the relative ordering of the Allred–Rochow electronegativities for As (2.20) and P (2.06) [40], as was previously noted in a comparative XPS study of binary transition-metal phosphides vs. arsenides [41].

### 3.3. Charge transfer within and between [ZrSi] and [CuPn] layers

It is useful to summarize the conclusions reached so far. The [ZrSi] layer contains Zr cations and Si anions, but the charges are not extreme (as implied by little or even no energy shifts relative to the element) and there is evidence for electronic delocalization. The [Cu*Pn*] layer contains $Cu^{1+}$ cations and *Pn* anions, with more pronounced energy shifts, consistent with a greater ionic character in the Cu–*Pn* bonds than in the Zr–Si bonds. Of the remaining questions, the most important is whether the separate layers interact; that is, we want to address the possibility that the *Pn* atoms are bonded not only to the Cu atoms, but also to the Zr atoms (Fig. 1b). If so, then it is of interest to determine how the extent of Zr–to–*Pn* or Cu–to–*Pn* charge transfer is altered in ZrCuSiAs vs. ZrCuSiP. Because transitions in Zr and Cu XANES spectra can reflect changes in the occupancy of specific states within atoms, they provide a way to answer these questions.

The Zr K-edge spectra reveal transitions of 1*s* electrons into unoccupied *p* states (Fig. 6a). The immediate observation that the spectra differ for ZrCuSiAs and ZrCuSiP implies that the Zr and *Pn* atoms do interact. We use the calculated conduction band for ZrCuSiAs (Fig. 7) to aid in the interpretation of these spectra by identifying qualitatively what orbital contributions are likely in the final states of these transitions. (The calculated conduction band for ZrCuSiP is similar and not shown here.) Peak A is assigned as a transition from Zr 1*s* to Zr 5*p* states that are hybridized with *p* states of Si and *Pn* atoms. This peak is more intense in ZrCuSiAs than in ZrCuSiP, which indicates that there are more pnicogen-based conduction states available in the former, consistent with the earlier assertion that As is less electronegative

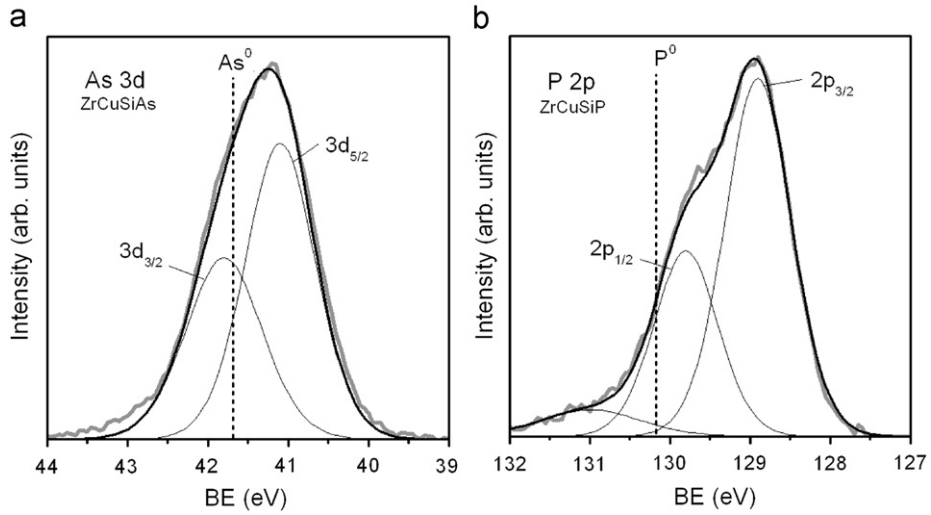


**Fig. 5.** (a) As 3*d* XPS spectrum, fitted with $3d_{5/2}$ and $3d_{3/2}$ components, for ZrCuSiAs, and (b) P 2*p* XPS spectrum, fitted with $2p_{3/2}$ and $2p_{1/2}$ components, for ZrCuSiP. The vertical dashed lines mark the As $3d_{5/2}$ BE for elemental As and the P $2p_{3/2}$ BE for elemental P.

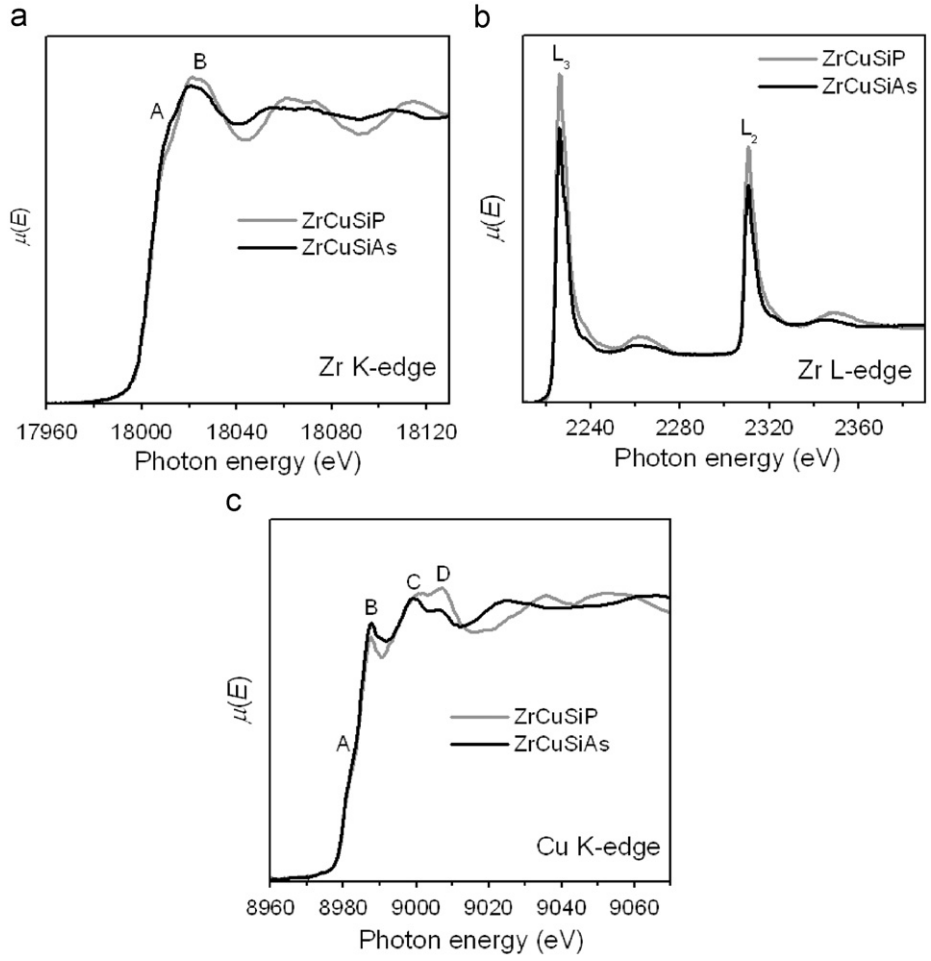


**Fig. 6.** Normalized (a) Zr K-edge, (b) Zr L-edge, and (c) Cu K-edge XANES spectra for ZrCuSiAs and ZrCuSiP. Zr and Cu K-edge spectra were measured in transmission mode and Zr L-edge spectra in TEY mode. Marked features are discussed in Section 3.3.

than P and thus that charge transfer is less from Zr to As than to P atoms. (An alternative assignment, an MSR phenomenon in which the peak becomes more intense with larger next-nearest neighbour atoms [42], can be dismissed because the second coordination sphere around Zr is the same in both compounds.) Peak B is assigned either as a transition from Zr 1*s* to Zr 5*p* states that are hybridized with Cu 4*p* states, or possibly an MSR process [42]. More convincing evidence for the interaction of Zr and *Pn* atoms is provided by the Zr L-edge spectra, which probe the Zr 4*d* states directly involved in bonding. Here, the spectra consist of

$L_3$- and $L_2$-edges, corresponding to transitions from Zr $2p_{3/2}$ and $2p_{1/2}$ states, respectively, to unoccupied 4*d* states (Fig. 6b). Both edges are less prominent in ZrCuSiAs than in ZrCuSiP, indicating that there are fewer Zr-based conduction states in the former.

Complementary information about the extent of metal-to-pnicogen charge transfer can be gained from the Cu K-edge XANES spectra, which reveal transitions of Cu 1*s* electrons into unoccupied p states (Fig. 6c). Peak A resembles a pre-edge feature corresponding to a dipole-forbidden $1s \rightarrow 3d$ transition commonly found for $Cu^{2+}$ species by virtue of their unfilled 3*d*-based conduction states [43]. Because the possibility of $Cu^{2+}$ was already eliminated from the XPS data, the more likely assignment is a dipole-allowed transition from Cu 1*s* to strongly hybridized Cu 3*d*/4*p* states associated with the tetrahedral coordination geometry around $Cu^{1+}$ species (similar to the case of copper(I) halides) [44]. An alternative assignment is a transition from Cu 1*s* to Cu 4*p* states that are hybridized with Zr 4*d* states, as found near the Fermi edge in the conduction band (Fig. 7). Although the Zr and Cu atoms are more than 3 Å apart, similar types of long-distance interactions have been implicated in the spectra of $Ca_{2-x}Sr_xFe_2O_5$ [45], $LaFeAsO_{1-x}F_x$ [46], and $La_2CuO_4$ [47]. Peak B is assigned as a transition from Cu 1*s* to Si 3*p* and *Pn np* states. With the assumption that the contribution from the Si states is identical (on the basis of the lack of changes in the Si XPS and XANES spectra), the greater intensity of this peak in ZrCuSiAs than in ZrCuSiP confirms that there are more pnicogen-based conduction states in the former. As before, this implies that As is less electronegative than P and that charge transfer is less from Cu to As than to P atoms. The remaining peaks, C and D, are assigned as transitions from Cu 1*s* to Zr 5*p* and Cu 4*p* states (seen in the conduction band), or possibly as MSR phenomena [48].

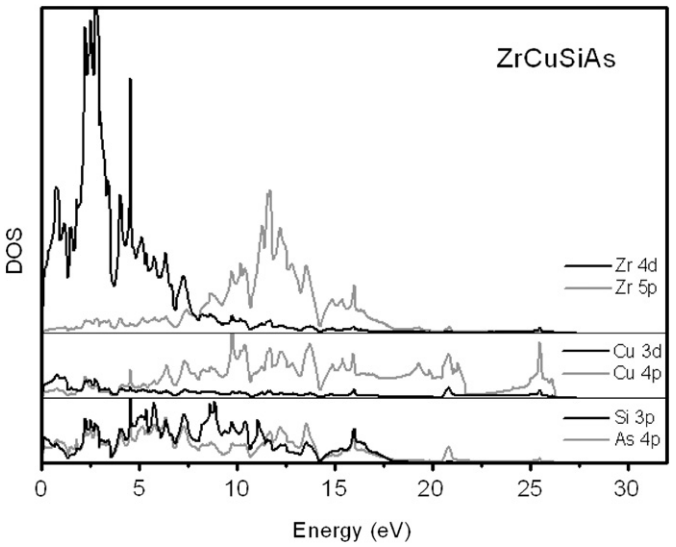


**Fig. 7.** Orbital projections of the calculated conduction states for ZrCuSiAs. The projections are offset for clarity but are set on the same scale.

### 3.4. Band structure

It is now of interest to see if the conclusions gained from the spectroscopic evidence are supported by the calculated band structure for ZrCuSiAs, in comparison to a representative rare-earth arsenide oxide, LaNiAsO. In common with other

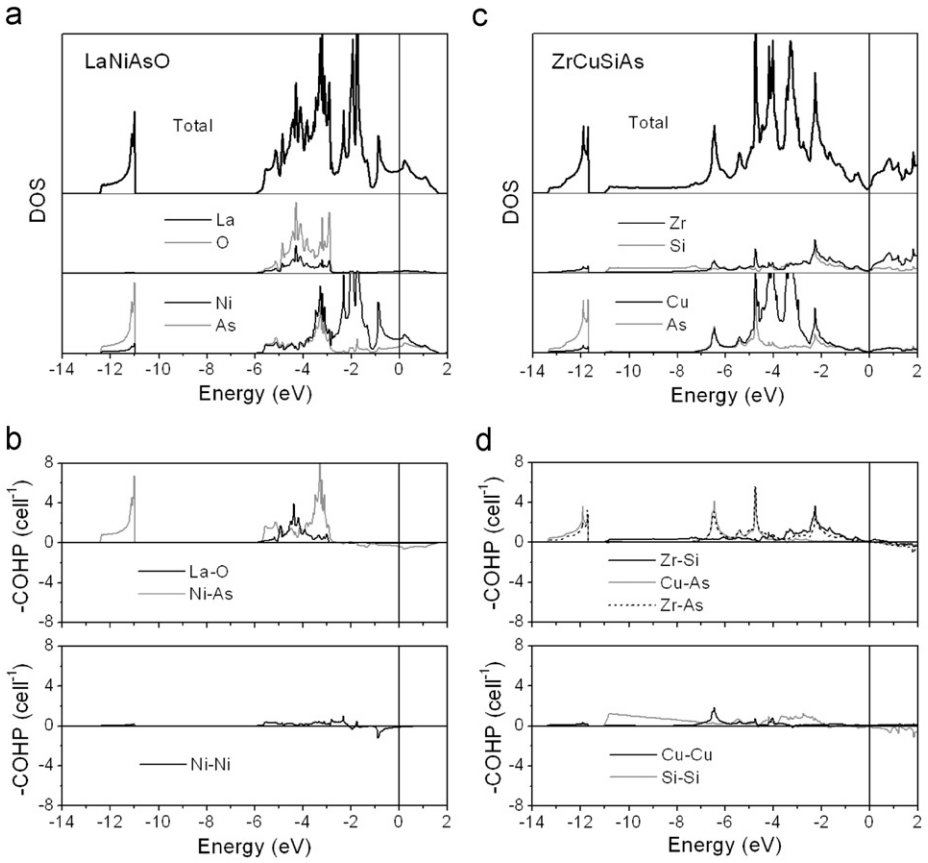


**Fig. 8.** Density of states (DOS) with its orbital projections and crystal orbital Hamilton population (COHP) curves for (a, b) LaNiAsO and (c, d) ZrCuSiAs. The Fermi level is at 0 eV.

rare-earth pnictide oxides, the band structure for LaNiAsO is characterized by a partially filled valence band that comprises a narrow range of La- and O-based states (from −6 to −3 eV) and a wider range of Ni- and As-based states (from −6 eV upwards), with the bands near the Fermi level dominated by Ni 3*d* states (Fig. 8a). (The narrow low-energy band centred near −11.5 eV largely comprises As 4*s* states.) Notwithstanding the usual assumption that the [LaO] layer contains ionic bonds [5], the mixing of La and O states implies that there is also some covalent character here, as reflected by the modest integrated crystal orbital Hamilton population (–ICOHP) value of 0.65 eV/bond and the occupation of La–O bonding levels in this energy range (Fig. 8b). The main stabilizing contribution in this structure, however, occurs within the [NiAs] layer, where a large –ICOHP of 1.88 eV/bond for the Ni–As contacts is derived from the occupation of strongly bonding levels. Weak Ni–Ni bonding (–ICOHP of 0.17 eV/bond) is associated with the arrangement of Ni atoms 2.92 Å apart forming square nets within the [NiAs] layer. The corresponding arrangement of O atoms, too far apart at 2.92 Å, within the [LaO] layer leads to no O–O bonding interactions (–ICOHP of 0.02 eV/bond), of course. If the interaction between La and As atoms is interrogated, the small (but non-negligible) –ICOHP value of 0.10 eV/bond indicates that interlayer bonding between the [LaO] and [NiAs] layers is considerably weaker than intralayer bonding; the picture of nearly separate ionic [LaO] and covalent [NiAs] layers holds.

The band structure for ZrCuSiAs reveals some striking differences (Fig. 8c). The Fermi level falls in a pseudogap, so that semimetallic behaviour is predicted. (Although the properties of ZrCuSiAs have not been measured, the electrical resistivity of ZrCuSiP is quite high, $1.5\times10^{-3}\,\Omega$ cm at 300 K, and falls only to $1.0\times10^{-3}\,\Omega$ cm at 5 K [8].) Unlike the [LaO] layer in LaNiAsO, the [ZrSi] layer gives rise to dramatically wider energy dispersion, consistent with more pronounced covalent bonding character associated with the occupation of Zr–Si bonding levels (–ICOHP of 1.51 eV/bond) (Fig. 8d). A wide subband extending down to −11 eV originates from orbital interactions of Si-based states, made possible by the closer 2.60 Å separation of Si atoms within square nets in the [ZrSi] layer. Occupation of Si–Si bonding levels leads to a substantial –ICOHP of 1.41 eV/bond, confirming the presence of strong delocalized homoatomic bonding within these polyanionic Si square nets. Relative to the [NiAs] layer in LaNiAsO, the compression of the [CuAs] layer in ZrCuSiAs within the *ab* plane does not alter the metal-arsenic bonding too much (–ICOHP of 1.43 eV per Cu–As bond) but does enhance the metal–metal bonding (–ICOHP of 0.49 eV per Cu–Cu bond). Importantly, the occupation of Zr–As bonding levels leads to substantial interlayer bonding (–ICOHP of 1.73 eV/bond) that is of the same magnitude as the intralayer bonding. Consistent with the Zr XANES spectra which show evidence for Zr–As interactions, the picture of interacting [ZrSi] and [CuAs] layers is confirmed.

## 4. Conclusions

A comparison of XPS and XANES spectra reveals profound differences that reflect the enhancement of covalent character on progressing from LaNiAsO to ZrCuSiAs. The [LaO] layer in LaNiAsO exhibits significant ionic character, as indicated by its O 1*s* BE which falls in the range expected for normal oxides, whereas the [ZrSi] layer in ZrCuSiAs exhibits strongly covalent character, as indicated by its Si 2*p* BE which is nearly the same as in elemental Si and is consistent with the development of a polyanionic Si network. The [NiAs] layer in LaNiAsO and the [CuAs] layer in ZrCuSiAs are similar in nature, with As $3d_{5/2}$ BEs slightly lower than in elemental As, indicating the presence of anionic As atoms and highly covalent *M*–As bonds. The [LaO] and [NiAs] layers in LaNiAsO can be treated independently (as suggested by the insensitivity of the As 3*d* BEs upon substitution of La with other *RE* elements), but the [ZrSi] and [CuAs] layers in ZrCuSiAs are strongly interacting (as suggested by the visible changes in the Zr K- and L-edge XANES spectra upon substitution of As with P). That is, there exists a real charge transfer from Zr atoms in the [ZrSi] layer to the As atoms in the [CuAs] layer. As inferred from shifts in the Zr K- and L-edge absorption energies, this metal-to-pnicogen charge transfer is enhanced even more in ZrCuSiP, indicating that P is more electronegative than As (in contradiction to tabulated Allred–Rochow values). Band structure calculations confirm that Si–Si and Zr–As interactions are ultimately responsible for the development of a three-dimensional covalent bonding network in ZrCuSiAs, in contrast to the two-dimensional character in LaNiAsO. The isolation of insulating (ionic) and conducting (covalent) layers is believed to be important in imparting the superconducting behaviour of the layered pnictide oxides. Strengthening the interactions between these layers can lead to changes in electronic structure that are manifested, for example, by smaller optical band gaps in β-PrZnPO than in α-PrZnPO [49,50]. It may be interesting to think of ways of tuning the transition from two- to three-dimensional character, something that appears to be feasible with this structure type.

## Acknowledgments

This work was supported through Discovery Grants to A.M. and R.G.C. from the Natural Sciences and Engineering Research Council (NSERC) of Canada. P.E.R.B thanks NSERC, Alberta Ingenuity, and the University of Alberta for scholarship support. Access to the Kratos AXIS 165 XPS spectrometer was provided by the Alberta Centre for Surface Engineering and Science (ACSES), which was established with support from the Canada Foundation for Innovation (CFI) and Alberta Innovation and Science. We thank Mr. Thomas Regier (SGM beamline), Dr. Lucia Zuin (PGM beamline), and Dr. Yongfeng Hu (PGM and SXRMB beamlines) for assistance with the XANES experiments conducted at the CLS, which is supported by NSERC, NRC, CIHR, and the University of Saskatchewan. We thank Dr. Robert Gordon for assistance with the Zr and Cu XANES experiments at PNC/XOR-CAT facilities at the APS. The PNC/XOR facilities are supported by the US Department of Energy—Basic Energy Sciences, a major research support grant (MRS) from NSERC, the University of Washington, Simon Fraser University, and the APS. The APS is also supported by the US Department of Energy, Office of Science, Office of Basic Energy Sciences, under Contract DE-AC02-06CH11357.

## Appendix A. Supplementary materials

Supplementary data associated with this article can be found in the online version at doi:10.1016/j.jssc.2010.04.032.

## References

[1] R. Pöttgen, D. Johrendt, Z. Naturforsch. B 63 (2008) 1135–1148.
[2] B.I. Zimmer, W. Jeitschko, J.H. Albering, R. Glaum, M. Reehuis, J. Alloys Compd. 229 (1995) 238–242.
[3] Y.-W. Ma, Z.-S. Gao, L. Wang, Y.-P. Qi, D.-L. Wang, X.-P. Zhang, Chin. Phys. Lett. 26 (2009) 037401-1–037401-4.
[4] Z.A. Ren, J. Yang, W. Lu, W. Yi, G.C. Che, X.L. Dong, L.L. Sun, Z.X. Zhao, Mater. Res. Innov. 12 (2008) 105–106.
[5] H. Takahashi, K. Igawa, K. Arii, Y. Kamihara, M. Hirano, H. Hosono, Nature 453 (2008) 376–378.

[6] H. Hiramatsu, H. Yanagi, T. Kamiya, K. Ueda, M. Hirano, H. Hosono, Chem. Mater. 20 (2008) 326–334.
[7] V. Johnson, W. Jeitschko, J. Solid State Chem. 11 (1974) 161–166.
[8] H. Abe, K. Yoshii, J. Solid State Chem. 165 (2002) 372–374.
[9] P.E.R. Blanchard, B.R. Slater, R.G. Cavell, A. Mar, A.P. Grosvenor, Solid State Sci. 12 (2009) 50–58.
[10] D. Briggs, Surface Analysis of Polymers by XPS and Static SIMS, Cambridge University Press, Cambridge, 2005.
[11] N. Fairley, CasaXPS, Version 2.3.9, Casa Software Ltd., Teighnmouth, Devon, UK, 2003 〈www.casaxps.com〉.
[12] G. Canning, M. Kasrai, G.M. Bancroft, D. Andrew, J. Synchrotron Radiat. 6 (1999) 740–742.
[13] B. Ravel, M. Newville, J. Synchrotron Radiat. 12 (2005) 537–541.
[14] R. Tank, O. Jepsen, A. Burkhardt, O.K. Andersen, TB-LMTO-ASA Program, Version 4.7, Max Planck Institut für Festkörperforschung, Stuttgart, Germany, 1998.
[15] C.D. Wagner, A.V. Naumkin, A. Kraut-Vass, J.W. Allison, C.J. Powell, J.R. Rumble Jr., NIST X-ray Photoelectron Spectroscopy Database, Version 3.5 (web version), National Institute of Standards and Technology, Gaithersburg, MD, 2003 〈srdata.nist.gov/xps〉.
[16] S. Doniach, M. Šunjić, J. Phys. C: Solid State Phys. 3 (1970) 285–291.
[17] A.P. Grosvenor, R.G. Cavell, A. Mar, R.I.R. Blyth, J. Solid State Chem. 180 (2007) 2670–2681.
[18] M.W. Gaultois, A.P. Grosvenor, P.E.R. Blanchard, A. Mar, J. Alloys Compd. 492 (2009) 19–25.
[19] R.L. Opila, G.D. Wilk, M.A. Alam, R.B. van Dover, B.W. Busch, Appl. Phys. Lett. 81 (2002) 1788–1790.
[20] D. Li, G.M. Bancroft, M. Kasrai, M.E. Fleet, X.H. Feng, K.H. Tan, B.X. Yang, Solid State Commun. 87 (1993) 613–617.
[21] M. Kasrai, W.N. Lennard, R.W. Brunner, G.M. Bancroft, J.A. Bardwell, K.H. Tan, Appl. Surf. Sci. 99 (1996) 303–312.
[22] D.C. Frost, A. Ishitani, C.A. McDowell, Mol. Phys. 24 (1972) 861–877.
[23] T. Ghodselahi, M.A. Vesaghi, A. Shafiekhani, A. Baghizadeh, M. Lameii, Appl. Surf. Sci. 255 (2008) 2730–2734.
[24] A. Rosencwaig, G.K. Wertheim, J. Electron Spectrosc. Relat. Phenom. 1 (1972/73) 493–496.
[25] A. Roberts, D. Engelberg, Y. Liu, G.E. Thompson, M.R. Alexander, Surf. Interface Anal. 33 (2002) 697–703.
[26] F. Werfel, M. Heinonen, E. Suoninen, Z. Phys. B: Condens. Matter 70 (1988) 317–322.
[27] R.P. Vasquez, Surf. Sci. Spectra 2 (1993) 144–148.
[28] R.P. Vasquez, Surf. Sci. Spectra 2 (1993) 149–154.
[29] S.K. Chawla, N. Sankarraman, J.H. Payer, J. Electron Spectrosc. Relat. Phenom. 61 (1992) 1–18.
[30] A. Kowalczyk, T. Toliński, M. Reiffers, M. Pugaczowa-Michalska, G. Chełkowska E. Gažo, J. Phys.: Condens. Matter 20 (2008) 255252-1–255252-7.
[31] P.C. Healy, S. Myhra, A.M. Stewart, Jpn. J. Appl. Phys. 26 (1987) L1884–L1887.
[32] H. Ishii, T. Koshizawa, T. Hanyu, S. Yamaguchi, Jpn. J. Appl. Phys. 32 (1993) 1070–1076.
[33] J. Sugiyama, R. Itti, H. Yamauchi, N. Koshizuka, S. Tanaka, Phys. Rev. B 45 (1992) 4952–4956.
[34] R.P. Vasquez, M.P. Siegal, D.L. Overmyer, Z.F. Ren, J.Y. Lao, J.H. Wang, Phys. Rev. B 60 (1999) 4309–4319.
[35] P. Steiner, V. Kinsinger, I. Sander, B. Siegwart, S. Hüfner, C. Politis, Z. Phys. B: Condens. Matter 67 (1987) 19–23.
[36] A. Bianconi, A. Congiu Castellano, M. De Santis, P. Rudolf, P. Lagarde A.M. Flank, A. Marcelli, Solid State Commun. 63 (1987) 1009–1013.
[37] J.-H. Choy, S.-H. Choi, S.-H. Byeon, S.-H. Chun, S.-T. Hong, D.-Y. Jung W.-Y. Choe, Y.-W. Park, Bull. Korean Chem. Soc. 9 (1988) 289–291.
[38] R.A.D. Pattrick, G. van der Laan, J.M. Charnock, B.A. Grguric, Am. Mineral. 89 (2004) 541–546.
[39] A. Siokou, M. Kalyva, S.N. Yannopoulos, M. Frumar, P. Němee, J. Phys.: Condens. Matter 18 (2006) 5525–5534.
[40] A.L. Allred, E.G. Rochow, J. Inorg. Nucl. Chem. 5 (1958) 264–268.
[41] A.P. Grosvenor, R.G. Cavell, A. Mar, J. Solid State Chem. 181 (2008) 2549–2558.
[42] F. Farges, S. Rossano, Eur. J. Mineral. 12 (2000) 1093–1107.
[43] J.M. Brown, L. Powers, B. Kincaid, J.A. Larrabee, T.G. Spiro, J. Am. Chem. Soc. 102 (1980) 4210–4216.
[44] T. Chattopadhyay, A.R. Chetal, J. Phys. C: Solid State Phys. 18 (1985) 5373–5378.
[45] A.P. Grosvenor, J.E. Greedan, J. Phys. Chem. C 113 (2009) 11366–11372.
[46] A. Koitzsch, D. Inosov, J. Fink, M. Knupfer, H. Eschrig, S.V. Borisenko, G. Behr, A. Köhler, J. Werner, B. Büchner, R. Follath, H.A. Dürr, Phys. Rev. B 78 (2008) 180506-1–180506-4.
[47] S.K. Pandey, S. Khalid, A.V. Pimpale, J. Phys.: Condens. Matter 19 (2007) 036212-1–036212-16.
[48] J.E. Penner-Hahn, Coord. Chem. Rev. 190–192 (1999) 1101–1123.
[49] H. Lincke, T. Nilges, R. Pöttgen, Z. Anorg. Allg. Chem. 632 (2006) 1804–1808.
[50] H. Lincke, R. Glaum, V. Dittrich, M. Tegel, D. Johrendt, W. Hermes, M.H. Möller T. Nilges, R. Pöttgen, Z. Anorg. Allg. Chem. 634 (2008) 1339–1348.